Am J Physiol Lung Cell Mol Physiol 315: L910–L918, 2018.
First published September 13, 2018; doi:10.1152/ajplung.00274.2018.

INNOVATIVE METHODOLOGY

Buffer drains and mucus is transported upward in a tilted mucus clearance assay

Jerome Carpenter,[1,2] Suzanne E. Lynch,[3] Jeremy A. Cribb,[4] Schuyler Kylstra,[4] David B. Hill,[2,4] and Richard Superfine[5]

[1]*Department of Pathology and Laboratory Medicine, The University of North Carolina, Chapel Hill, North Carolina;* [2]*Marsico Lung Institute, The University of North Carolina, Chapel Hill, North Carolina;* [3]*Department of Biochemistry and Biophysics, The University of North Carolina, Chapel Hill, North Carolina;* [4]*Department of Physics and Astronomy, The University of North Carolina, Chapel Hill, North Carolina; and* [5]*Department of Applied Physical Sciences, The University of North Carolina, Chapel Hill, North Carolina*

Submitted 12 June 2018; accepted in final form 27 August 2018

Carpenter J, Lynch SE, Cribb JA, Kylstra S, Hill DB, Superfine R. Buffer drains and mucus is transported upward in a tilted mucus clearance assay. *Am J Physiol Lung Cell Mol Physiol* 315: L910–L918, 2018. First published September 13, 2018; doi:10.1152/ajplung.00274.2018.—Mucociliary clearance (MCC) plays an essential role in maintaining airway sterility and health. Conversely, mucociliary dysfunction is implicated across many airway obstructive diseases. Understanding the necessary requirements for successful MCC is imperative to establish the pathology of disease, as well as to develop therapeutic strategies. Although postural, that is, gravitational, drainage is used clinically to aid mucus clearance, it is ignored in both animal and cell culture models of MCC. In this study, we develop a novel mucus clearance assay that enables the first particle image velocimetry of human bronchial epithelial cell cultures tilted relative to the gravitational field. This tilting system makes it possible to observe drainage of the airway surface liquid and, thus, reveals the effect gravity has on mucociliary clearance. First, we use this assay to demonstrate that beating cilia alone cannot transport buffer upward against gravity. Next, we show the same cilia successfully transporting mucus upward. These results indicate that the biophysical and biochemical properties of mucus enable vertical clearance and that current assay systems are not equipped to determine which properties are required for physiologically relevant vertical mucociliary clearance.

drainage; mucociliary clearance; mucus clearance assay; organ on a chip; tilting microscope

INTRODUCTION

Mucociliary clearance (MCC) serves an essential role in maintaining airway sterility and health. The healthy airway uses a mucosal barrier to trap and remove toxicants and pathogens (32). Mucosal flow transports these trapped foreign bodies out of the airway through cough (31) or the coordinated activity of cilia. When mucus clearance fails, the airway becomes vulnerable to infection and inflammation, a combination that can severely compromise lung function. Failed or diminished MCC is part of the pathology of several airway diseases, including chronic obstructive pulmonary disease (COPD), cystic fibrosis (CF), respiratory infections, and asthma. COPD and lower respiratory infections alone are responsible for more than 7 million deaths per year worldwide (38). Thus, understanding the parameters that differentiate between healthy and failed clearance is of paramount importance in assessing and treating lung diseases. At a fundamental level, many questions remain about cilia-driven clearance, especially with regard to the rheological and biochemical parameters of mucus that enable successful long-distance transport despite the biophysical challenges presented by the human lung.

A variety of model systems, both animal and in vitro, have been employed to study several aspects of MCC. Several animal models have been developed to study MCC in diseased states, including murine models for primary ciliary dyskinesia (43) and CF (56) and porcine models for CF (21). Ex vivo preparations, such as frog palates, have been used by several different groups to establish relationships between mucus rheology and airway surface liquid (ASL) transport (9, 15, 30, 46, 47), and more recently, ferret (27) and pig (2) tracheas have been used for mucociliary transport studies. In vitro models possess several attractive features, including the ability to study phenomena under high-quality microscopy and to carefully control experimental conditions. The development of the air-liquid interface (ALI) cell culture model (5, 16) has enabled detailed study of several aspects of mucociliary clearance, which include the periciliary liquid layer (39), the glycocalyx/membrane mucins (8, 28), mucus and cilia interactions (35), and mucus-epithelial tethering (7, 50). Subsequent studies have integrated the ALI model with flow and microfluidics chambers to understand the interplay between fluids and the epithelium (12), to model the fluid mechanical stress of a rupturing liquid plug in the small airways (23), and later incorporated substrate stretching and used the system to study inflammatory response to nanoparticles, and mechanosensitivity of alveolar cells (24). Recent systems by Sellgren et al. (51) and Benam et al. (3) have advanced physiological relevance by coculturing with endothelial cells and fibroblasts, as well as developing a cell culture model of inflammatory lung diseases, respectively. However, a major factor ignored in animal models, as well as in vitro models studying mucus clearance to date, has been drainage due to gravity.

Address for reprint requests and other correspondence: R. Superfine, Applied Physical Sciences, The Univ. of North Carolina, Chapel Hill, NC, 27599-3050. (e-mail: superfine@unc.edu).

We are especially interested in the challenge of propelling mucus upward against gravity as occurs throughout the lung, especially in the upper airway of an upright person. Even when supine, the complex geometry of the lung (54) guarantees that portions of the lower lung will also require transport against gravity. Also of interest, the therapeutic method of postural drainage is predicated on the ubiquitous role of gravity in promoting drainage (13, 40, 55). Although it may be true that factors other than gravity might contribute to the efficacy of postural drainage (33), it is important to determine the role of gravity in MCC in both healthy and diseased states. Wong et al. (55) demonstrated normal patients with effective clearance in both head-up and head-down (−25° tilt) positions, while CF patients experienced dramatic changes dependent on body orientation. All CF patients showed increased cephalad (toward the head) flows when tilted to a head-down position, with half of the patients showing a complete reversal of flow direction when upright. These latter patients regularly showed bolus flows in the direction of the lung when upright. We conclude that mucus drainage due to gravity is well established in human patients and that gravity may overcome cephalad ciliary propulsion in diseased states. To understand the conditions that promote and maintain homeostasis, we use a novel vertical clearance assay to understand the biophysical and biochemical conditions that allow cilia-mediated flows to overcome gravity.

In this study, we present a vertical mucus clearance assay that combines a microfluidic platform, which supports well-differentiated, well-ciliated human bronchial epithelial cells (HBECs), with a tilting microscope. Moving beyond prior work, we have achieved cilia-generated mucus flow over long range within a technology suitable for a variety of controlled in vitro studies. We place this system on a microscope mounted on a tilt table that allows high-resolution microscopy and particle image velocimetry (PIV), while challenging cilia-driven flows to overcome gravitational drainage. By performing the first PIV measurements in a tilted in vitro system, we successfully demonstrate cessation of transport in a liquid (buffer) as a function of gravitational drainage. Conversely, mucus successfully transports upward at 30, 45, 60, and even vertically at a 90° tilt angle. This difference further demonstrates that gravitational drainage plays an essential role in clearance and must be included when evaluating biochemical and rheological parameters that govern mucociliary clearance.

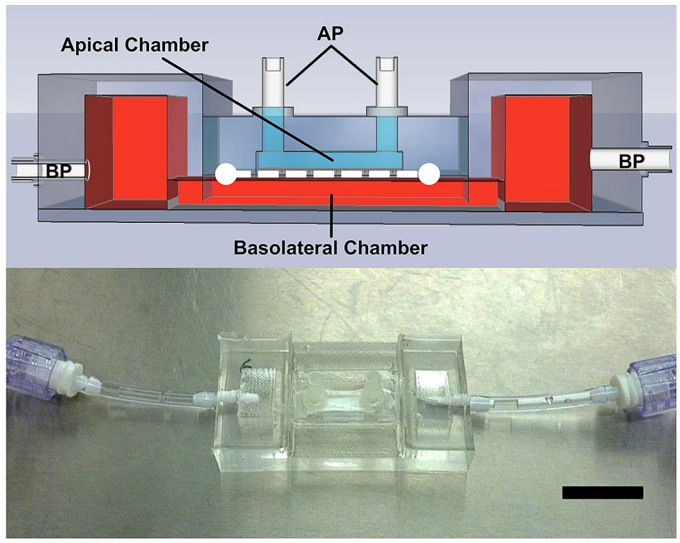

Fig. 1. *Top*: cross section of the mucus clearance assay device (MCAD). The basolateral chamber is colored in red, while the apical chamber is colored in light blue. Apical access ports are marked AP, and basolateral access ports are marked BP. Dimensions of the apical chamber are 20 mm × 5 mm × 0.2 mm. The basolateral chamber spans the area of the apical channel and has a height of 0.4 mm. *Bottom*: completed mucus clearance assay device. Tubing and valves have been connected to the basolateral ports. Scale bar: 20 mm.

MATERIALS AND METHODS

Fabricating the mucus clearance assay device. The mucus clearance assay device (MCAD) consists of two separate units: a basolateral compartment to house media and an apical chamber for cell growth (Fig. 1) Each unit was fabricated by casting polydimethylsiloxane (PDMS) into custom acrylonitrile-butadiene-styrene plastic and acrylic molds. The apical compartment was created using a two-step molding process (Fig. 2) and apical access ports were added as detailed by Liu and Moiseeva (36). A commercially available Millicell scaffold (Millipore PICM3050) served as the bottom of the apical chamber and the cell-growing surface. The completed apical chamber had a cell-growing area of 20 mm × 5 mm, with a height of 200 μm for cells and apical fluid. The basolateral chamber was fabricated and attached to the bottom of the apical compartment (Fig. 2).

Sterilization and channel preparation. MCADs were sterilized with ethylene oxide (EO) gas and then ventilated in a sterile environment to dissipate any accumulated EO. The apical compartments were next treated with collagen type IV (Sigma C-7521) as prepared by Fulcher et al. (14). We pipetted 100 μl of the collagen solution atop the Millicell scaffold and let it dry overnight. The next morning, any excess fluid was removed, and the channel was exposed to UV light for 30 min to facilitate binding of the collagen layer. External tubing and valves were sterilized with a 70% ethanol solution, rinsed with sterile PBS, and then attached to the MCAD.

Cell seeding and culture. Once passaged, normal HBECs and ALI media were provided by the University of North Carolina Cystic Fibrosis Tissue Procurement Core, as detailed by Fulcher et al. (14). Apical compartments of each MCAD were seeded with 250,000 cells, and then the apical ports were capped with PDMS to maintain sterility. The basolateral compartment was filled with 1 ml of ALI media, which was exchanged three times a week. The apical compartment was initially filled with media, which was exchanged three times a week. Once the cells reached 100% confluence, an ALI was maintained in the apical compartment; media were no longer added apically, and any accumulated fluid was pipetted out of the channels daily. Additionally, the apical compartment was washed with PBS weekly.

Calcein staining and cell confluence. Cell viability was assessed using a live/dead cell assay kit (Invitrogen: L3224). A PBS solution with 4 μM calcein-AM and 2 μM ethidium homodimer was pipetted into the apical compartment. After 15 min, the solution was removed from the channel and replaced with PBS. The channel was imaged as overlapping fields of view in both green and red fluorescent channels using an Olympus IX-81 with a CARVII spinning disk confocal system and Photometrics QuantEM camera. Images were processed using ImageJ (National Institutes of Health, Bethesda, MD) and then stitched into a panorama using Adobe Photoshop (Fig. 3).

Tilting the MCAD to study gravitational effects. To test the effects of gravity on MCC, we built a tilting microscope base (Fig. 4). Briefly, we designed and built an elevated platform capable of rotating azimuthally and locking into place at 0, 30, 45, 60, and 90° relative to its base. We then secured an Olympus IX-81 microscope to the elevated platform, and clamped the stage in place to lock its position as the microscope rotated in space. We then attached a micrometer-

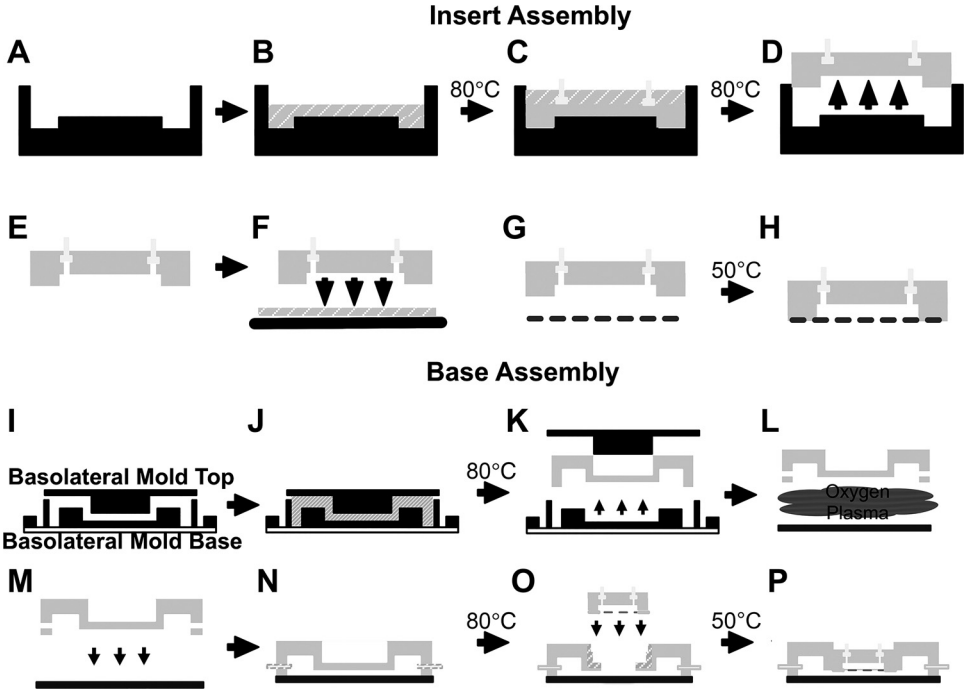

Fig. 2. Fabrication of the completed mucus clearance assay device (MCAD) device. *Top*: processing steps to mold the apical compartment of the MCAD. *A*: process starts with a custom acrylonitrile-butadiene-styrene plastic and acrylic mold. *B*: polydimethylsiloxane (PDMS) is poured into the mold and cured at 80°C for 1 h. *C*: screw insulators are placed on top of the cured PDMS, and additional PDMS is poured to embed the feet of the insulators. The added PDMS is cured at 80°C for 1 h. *D*: device is removed from the mold. *E*: holes are punched with a 2-mm biopsy punch to make a path through the screw insulator into the channel region. *F*: thin layer of PDMS is prepared via spin coating on a glass slide at 1,200 rpm for 60 s. The bottom of the channels is stamped into this thin PDMS layer. *G*: stamped channel is pressed onto a Millicell scaffold. *H*: channel is cured in the oven at 50°C for 2 h (the lower temperature is to prevent scaffold degradation). *Bottom*: *I*: starting with the combined acrylic/ acrylonitrile butadiene styrene plastic hybrid mold. *J*: PDMS was poured into the mold and cured at 80°C for 1 h. *K*: PDMS was removed from the mold assembly and a biopsy punch was used to make holes into the reservoir of the chamber. *L*: PDMS and a glass slide were both cleaned with isopropyl alcohol and methanol and exposed to a 10-W oxygen plasma, which activated both surfaces. *M*: activated PDMS was pressed against the activated glass slide to create a permanent irreversible bond. *N*: uncured PDMS was placed around 1/16″ hose barb adapter and placed into the reservoir holes. The system was then cured at 80°C for 1 h. *O*: basolateral chamber was "painted" with uncured PDMS, the apical compartment (see above) was lowered onto the uncured PDMS, and the entire assembly was cured at 50°C for 2 h to produce the completed mucus clearance assay device (*P*).

positioning stage, which allowed us to carefully maintain and translate the field of view. Instructions and drawings detailing platform design and assembly can be found in the supplemental section (Supplemental Figs. S1–S9). All experiments were performed with nonimmersion objectives, as there is the potential for immersion media drainage while tilting the scope. Using the tilting scope along with the bilayered MCAD allowed us to image cilia-driven fluid flow at various tilt angles while maintaining cell growth media basolaterally. Increasing the tilt angle, α, increased the component of the gravity vector parallel to the epithelium, which allowed fluid drainage in the apical compartment. Incorporating drainage into the chamber created three regions with distinct fluid environments (Fig. 4*B*). In *region 1*, the submerged region, the depth of the apical fluid exceeds the ability of the epithelium to absorb liquid. This environment models pulmonary edema, mucus plugs, or systems where excessive liquid exists on the apical surface. *Region 2*, the meniscal region, is a transitional area, where interactions between the apical fluid, epithelial surface and chamber walls dominate fluid height. Finally, several factors control apical fluid height in *region 3*, the air-liquid interface zone, including liquid drainage due to gravity, epithelial fluid absorption, and cilia-driven fluid transport. *Region 3* is unique among models in that it recreates the fluid environment found in vertically oriented regions of the lung. All experiments in this study were performed in the meniscal and ALI regions, as there is no definitive boundary between the two regions.

Tilted particle image velocimetry experiments. After establishing well-differentiated, well-ciliated cultures, we mapped the transport of endogenous material with the channel in a horizontal orientation. We then identified regions of interest based on two criteria. First, the region showed directed, cilia-driven flow of endogenous material along the axis of the channel (linear) or circularly (hurricane). Second, to avoid wetting effects, we ensured that the region was not adjacent to the channel sidewalls.

Before flow measurements, we removed endogenous material from the apical surface. Next, cells were washed with PBS and then incubated in a 50 μM ATP solution to release stored mucins. Cells were then washed in PBS again and exposed to a 10-mM dithiothreitol (DTT) solution to facilitate mucus removal (39, 50). Finally, the cells were washed in PBS a third time to remove any excess DTT and mucus.

We then tilted the microscope to 30° relative to the ground and affixed the MCAD onto the microscope stage (Fig. 4). Using a micrometer positioning stage, we set the microscope field of view to a previously identified region of interest.

The PBS was then removed from the apical compartment via a pipette from the "downhill" port. We next added a 0.01% wt/vol solution of 2-μm diameter beads suspended in either PBS or 2.5% reconstituted HBE mucus, as prepared by Hill et al. (20) to the downhill port using a pipette. Fluid was slowly added until the fluid contact line reached the region of interest. Videos were taken in the original field of view (the field with the original contact line), as well as fields of view "uphill" and "downhill" (traversing the long axis of the channel along the plane of the epithelial surface). Once all videos were taken for a particular tilt angle, we used the micrometer-positioning stage to return to the original field of view and then tilted

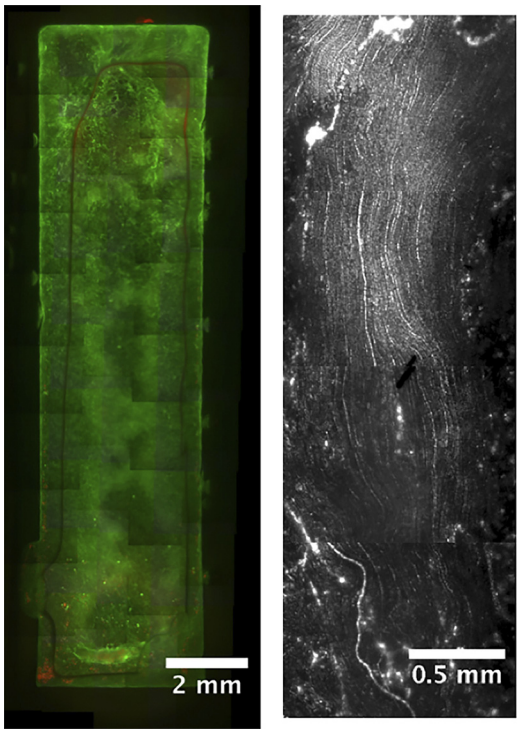

Fig. 3. Human bronchial epithelial (HBE) cells in the mucus clearance assay device (MCAD) span the entire channel and demonstrate long-range cilia-driven transport. *Left*: composite image showing a live/dead assay of an entire channel. Live cells show up as green, while dead cells are red. The majority of cells are alive, and they span the entire channel. *Right*: maximum intensity projection (MIP) of fluorescent bead transport in a MCA device. The MIP of the fluorescent beads represents pathlines of the cilia-driven flow. Frequently, devices had regions spanning more than a few millimeters where cilia-driven flow was aligned along the axis of the channel.

the microscope to the next angle of interest. Movies were captured using a JAI CM-30GE Pulnix camera recording at 90 frames/s.

Video analysis and PIV. Videos were imported into Video Spot Tracker (VST) software (Center for Computer Integrated Systems for Microscopy and Manipulation http://cismm.web.unc.edu) and tracked using the symmetric kernel. Generally, the tracking parameters were tuned to maximize the number of tracked particles. Particle positions from VST were imported into MATLAB and filtered to remove particles that did not move during the course of the video. To determine the average number of particles as a function of uphill position, we segmented the field of view into rows and counted all of the moving particles in each row per video frame, before finally averaging over the video.

Determination of the mucus hurricanes' center of circulation and its movement required frame registration between videos and determination of the center of the hurricane. Frame registration was accomplished by using ImageJ to create a minimum intensity projection of each video. Stationary (stuck) particles, which served as fiducial markers, were the only features visible in the projection. The x,y coordinates of the fiducials were compared and used to correct any changes in the field of view between videos. This registration showed that the field of view did not shift for videos at the same tilt angle, and it was used to correct for minor field-of-view slippage that occurred during microscope tilting.

Determination of the mucus hurricane center of circulation was accomplished by using ImageJ to create a maximal intensity projection (MIP). Using the MIP, we identified a series of particle pathlines for each video. In an effort to better describe the system, pathlines roughly coinciding in the same ellipse were considered to be segments of that ellipse. Coordinates were chosen along the perimeter of the ellipse, and those coordinates were used in a least squares fitting method proposed by Halir and Flusser (17) and implemented in MATLAB (10). After creating several ellipses for each video, the average of the ellipse centers was calculated and compared against the video registration to determine the hurricane's movement as a function of tilt angle.

Determining cilia beat frequency. Cilia beat frequency (CBF) was determined by taking phase contrast videos of the field of view and performing Fourier spectral analysis on each pixel as a function of time. Twenty-second videos were recorded at 90 frames/s using a JAI CM-30GE Pulnix camera and a ×40 objective. Videos were imported into MATLAB, where each pixel was stored as an array of grayscale values versus time. Each array was edge synchronized (a linear term was subtracted from the array members, so that the first and last array elements had the same grayscale value), windowed, and then transformed via fast Fourier transform. The dominant peak in the power spectrum was selected and checked against the next highest peaks (2.5 standard deviations away in power) to determine each pixel's light intensity fluctuation frequency and to make sure that the signal was distinct from the noise. Frequencies were reported for each pixel, and the average of all the pixels with nonzero frequencies was used to determine the CBF for a field of view.

RESULTS

Well-differentiated, well-ciliated cells in a fluidics channel. Cells grown in the MCAD demonstrated many of the same characteristics as cells grown using conventional HBE cell culture protocols. Cells remained highly viable and grew to 100% confluence across the entire device (Fig. 3); this serves as a demonstration of patterning the HBE cell cultures to form customized geometries. Furthermore, the cultures became well-differentiated, well-ciliated cultures within the confines of the geometry. Percent ciliation typically ranged between 40 and 60%, with dense areas of cilia that often exhibited millimeter-scale linear transport along the axis of the channel or

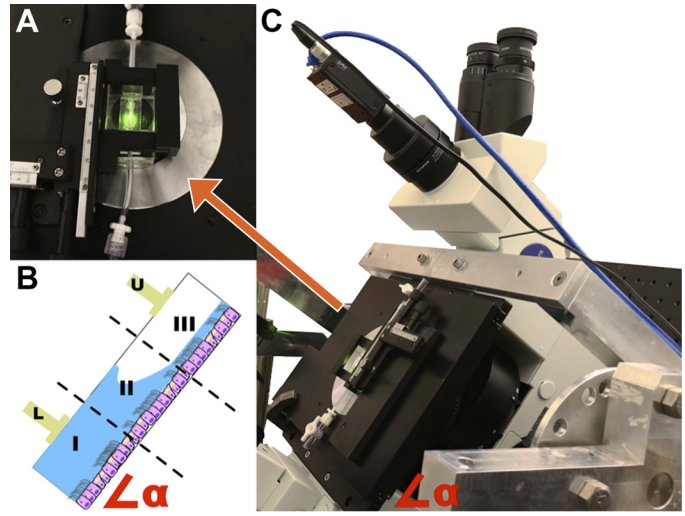

Fig. 4. The mucus clearance assay device (MCAD) loaded onto the tilting microscope. *A*: MCAD is pinned to the microscope platen and maneuvered with an x,y stage. *B*: cartoon showing the different regions of the MCAD when the system is tilted by angle α. Angle α is the angle between horizontal and the plane of the epithelial surface. L and U denote the lower and upper access ports of the MCA chamber, respectively. Region I is the submerged zone, region II is the meniscal zone, and region III is the air-liquid interface zone. *C*: MCAD affixed to the tilted microscope and rotated by angle α (60° in this image).

circular transport, such as the mucus hurricanes observed by Matsui et al. (39). Although not explicitly tested in this study, we did see evidence that the linear shape of the channel may have contributed to ciliary alignment along the axis of the channel.

Reconstituted 2.5% HBE mucus clears against gravity, buffer does not. To explore the relevance of gravity on ciliary clearance, we performed PIV measurements as a function of tilt angle with microbeads suspended in both PBS and reconstituted 2.5% mucus solutions (20). The latter is representative of healthy mucus. When performing the experiments, we swept through tilt angles starting at a 30° angle and ending with a vertical orientation (90°). In proceeding this way, we increased the magnitude of the gravitational component parallel to the epithelial surface (and simultaneously decreased the magnitude of the perpendicular component) The initial angle of 30° was chosen to prevent fluid added to the bottom of the system from moving beyond the meniscus without the aid of cilia-driven transport. Both the buffer and reconstituted mucus solutions were added, so that their initial contact lines coincided at 30°. We measured CBF at both the beginning and end of the experiment and found it to be ~13 Hz for both buffer and reconstituted mucus. In the case of buffer, the furthest uphill extent of freely moving fluorescent beads was the initial contact line; as tilt increased, the extent to which particles traveled uphill decreased (Fig. 5, *A*, *C*, *D*; Supplemental Video SV1). In the case of mucus, however, beads transported far past the meniscus regardless of tilt (Fig. 5, *B–D*; see Supplemental Videos SV2 and SV3), traveling at times more than a millimeter beyond the initial contact line. Figure 5*C* follows the average number of freely moving beads as a function of uphill distance in the channel for various tilt angles. In the buffer case, transport ceases as the liquid drains with increasing tilt. Conversely, transport continues against gravity in the mucus case, independent of tilt, with some drainage occurring due to heterogeneities in ciliation. Once cilia propel the fluid over nonciliated areas, it subsequently drains downhill. This drainage occurs to a greater extent at the lower tilt angles due to *1*) the fluid's ability to better accumulate in nonciliated regions at lower tilt angles before draining, and *2*) the tilt experiments are done in succession, so upon starting the experiment at 90°, fluid has already had the opportunity to drain. Because of this effect, the uphill bead velocity at the 90° tilt angle appears to be larger than other tilt angles in Fig. 5*D*, but we anticipate that this artifact would vanish in a fully ciliated system.

Mucus hurricanes maintain circulation in a vertical orientation. In addition to exploring the effect of gravity on cilia-driven flow over linearly coordinated cilia, we also explored the effect of drainage over cilia coordinated to move

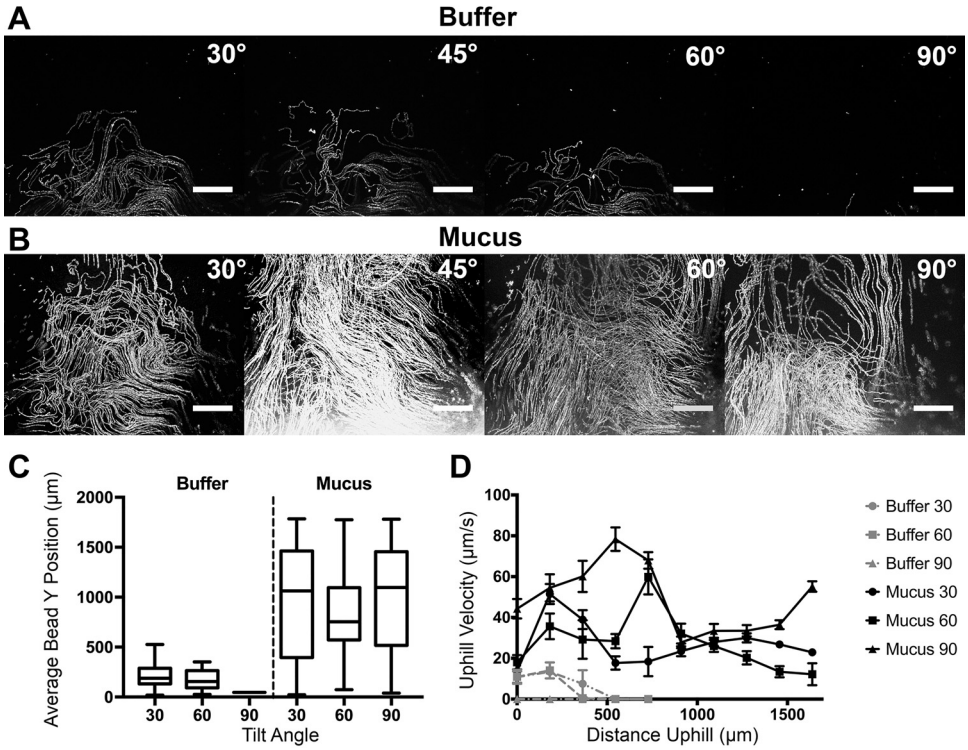

Fig. 5. Microbeads in buffer drain with increasing tilt angle, while microbeads in reconstituted mucus continue uphill, cilia-driven transport. *A*: maximum intensity projection (MIPs) representative of the pathlines of tracers suspended in buffer as a function of mucus clearance assay device (MCAD) tilt angle. The extent to which tracers travel uphill over the ciliated cells is reduced with increasing tilt angle. Scale bar: 200 μm. *B*: MIPs representative of the pathlines of tracers suspended in 2.5% reconstituted mucus as a function of MCAD tilt angle over the same region of cells in *A*. Particles in mucus continue to travel uphill beyond the meniscus at all tilt angles, including 90°. Scale bar: 200 μm. *C*: average "*y* position" (distance uphill from a common origin) for tracer beads in buffer and reconstituted mucus as a function of tilt angle. In buffer, beads are constrained to the meniscus region, which recedes downhill with increasing tilt angle. In mucus, beads have a range that spans both field of views observed (the initial field of view with the meniscus, as well as the uphill field of view) regardless of tilt angle. *D*: mean upward velocity of tracers being driven uphill by cilia at different distances uphill of a common origin in buffer and reconstituted mucus. Beads in the reconstituted buffer have a lower mean uphill velocity than beads in mucus, and upward bead transport stops in buffer uphill of the meniscus.

fluid in a rotational pattern. We examined the transport of a buffer-bead and mucus-bead solution as a function of tilt angle over the same field of cells. To dispel any concerns regarding the initial contact line of the two solutions, we biased the system so that the mucus contact line was well below the mucus hurricane. The mucus-bead solution transported uphill over the course of ~10 min to form the visible mucus rotational pattern known as a "hurricane" (39). In the buffer experiment, the initial contact line started above the circularly coordinated cilia and drained across them with increasing tilt angle (Supplemental Videos SV4 and SV5). An immediate difference between the mucus system and buffer system is the smoothness of the mucus system (Fig. 6; Supplemental Videos SV6 and SV7). Although the tracers are over the same field of view, the beads in buffer show much less coordination in their movement, an observation also made by Matsui et al. (39). Similar to the linear experiment, buffer transport was restricted to the region downhill of the contact line. As the system was tilted to increasing angles, bead transport retreated along with the contact line, leaving behind no rotational flow pattern after the lowering of the contact line. In the mucus system, however, the circular bead transport persisted through all tilt angles.

DISCUSSION

In this study, we designed and used a novel assay to demonstrate the importance of gravitational drainage in mucociliary clearance. Clearance/transport stopped as a function of increasing tilt angle in experiments where buffer was the only fluid above the cilia, ultimately resulting in fluid drainage. In contrast, upward transport of mucus continued regardless of tilt angle, even transporting upward at a tilt angle of 90°!

Our findings agree qualitatively with an MCC gravitational drainage model derived by Blake et al. (6), where a higher viscosity fluid successfully transports against gravity, while a lower viscosity fluid succumbs to drainage. Blake et al. (6) solved for the velocity profile as a function of tilt angle for the drainage of a mucosal layer sitting atop a serous layer:

$$U(z) = \frac{\rho g \sin(\alpha)}{4\mu} z(z - 2h), \qquad (1)$$

where $U(z)$ is fluid velocity at height z, z is the coordinate normal to the cell surface registered at the tips of the cilia (presumed here to be stationary), α is the tilt angle of the channel with respect to horizontal, h is the total depth of the liquid, g is the acceleration due to gravity, and ρ and μ are the ASL's density and viscosity, respectively. This relationship is derived from the Navier-Stokes equation, which assumes a steady and uniform flow, a fluid velocity entirely parallel to the epithelial surface, and no external pressure to the system.

Integrating over the z dimension and dividing by the total liquid depth, h, we can get an expression for U_{avg}, the average velocity of the fluid due to drainage only:

$$U_{avg} = -\frac{\rho g \sin(\alpha)}{6\mu} h^2 \qquad (2)$$

The drainage velocity is proportional to the square of the fluid depth and inversely proportional to fluid viscosity. The solution velocity here is always negative, indicating fluid drainage at all positive tilts and viscosities. Lower-viscosity fluids (i.e., buffer) drain faster than higher-viscosity fluids (i.e., mucus). Momentarily ignoring the contribution of cilia, we can use this simple model to determine the drainage velocity for buffer in our experiments as a function of tilt angle. Using the viscosity and density of water, 8.9×10^{-4} Pa·s and 1,000 kg/m^3, respectively, and choosing a buffer thickness of 10 μm, we can calculate that buffer would drain at 90 μm/s at a 30° tilt angle and at 180 μm/s for a 90° tilt angle.

Reintroducing an opposing, cilia-driven upward velocity U_{cilia} (at the cilia/fluid interface, $z = 0$), we have a new expression for the average fluid flow:

$$U_{avg} = -\frac{\rho g \sin(\alpha)}{6\mu} h^2 + U_{cilia} \qquad (3)$$

As an example, we can assume an upward cilia-driven velocity U_{cilia} of 80 μm/s, the highest value observed in the Matsui system (39) and approximately what Hussong et al. (25) observed in buffer 10 μm away from the cilia tips. Summing these velocities, we find that a 10-μm layer of buffer would slowly drain −10 μm/s, at 30°, and it would rapidly drain −100 μm/s, at 90°. This model does not preclude vertical buffer transport, but it does constrain the liquid depth at which net upward transport will occur. By setting the net velocity of *Eq. 3* equal to 0, we can solve for the maximum buffer thickness that cilia can transport vertically. The maximum supported fluid thickness is calculated to be 6.6 μm. However, we observe no upward bead transport even at tilt angles of 30°. Although we do not directly measure the thickness of our fluid layer, we can reasonably assume the observed layer thickness (in cases in which we do not observe any beads) is less than the 2-μm bead diameter. Therefore, we conclude that a no-slip boundary condition with an impenetrable boundary at the cilia-ASL height does not provide an accurate model for cilia-generated flows. This may be due to several factors.

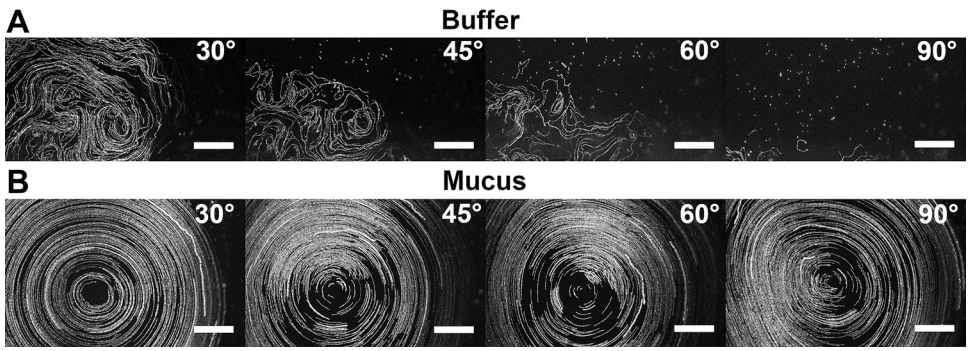

Fig. 6. Circularly cilia-driven systems (hurricanes) drain as a function of tilt angle in buffer but maintain circulation without draining in the case of reconstituted mucus. Maximum intensity projection (MIPs) represent the pathlines of fluorescent tracer particles as a function of tilt angle in buffer (*A*) and reconstituted 2.5% mucus (*B*). In buffer, transport is confined to the region below the liquid contact line. As tilt angle increases, and this line retreats due to drainage, the region capable of supporting bead transport diminishes. In mucus, transport is maintained regardless of tilt angle and even persists at a tilt angle of 90°.

First, ciliation is incomplete with interspersed regions of bare, unciliated cells. The upward shear stress provided by the ciliated cells may not properly overcome the drainage occurring over bare cells, and a mean field approximation may not be appropriate. Second, there is evidence that cilia-driven flow is minimal below the cilia tips (39, 52). This region may itself drain, and the fluid above the cilia tips may move vertically into the intercilia region. This is explicitly not included in Blake's model. It is certainly interesting that a shear flow boundary condition derived from flow observed in cell cultures oriented horizontally does not describe our observed phenomena in tilted cultures.

Our observation of buffer transporting over a region of cilia at a low tilt angle, but ceasing to transport at a steeper tilt angle provides direct experimental evidence of gravitational drainage affecting ciliary transport. There has been a recent report of mucus-free transport in a vertical configuration (4). However, that system is completely submerged and, therefore, does not allow for fluid drainage or for neutrally buoyant particles carried by any draining fluid. Physiologically, a submerged system would be applicable to a flooded lung region, whereas our model system is relevant to cilia-generated flows in open airways.

Similarly, we can use Blake's model to better understand the reconstituted mucus studies. Using our measured effective viscosity of 0.16 Pa·s, 1,000 kg/m^3 as the density of mucus [as used in Norton et al. (41) and Smith et al. (53)], and keeping the other parameters the same, we find a drainage rate of 0.5 μm/s at 30° and 1 μm/s at 90°. Therefore, in the case of a fluid with the viscosity of reconstituted mucus, the contributions of ciliary transport are enough to overcome the drainage velocity. If we again assume a no-slip traction layer boundary condition at the cilia-mucus interface, moving 80 μm/s up the channel, we find that cilia could support a 88-μm-thick layer of reconstituted 2.5% mucus, more than 10 times the thickness of a buffer layer. Moreover, this value is in line with the reports of ASL thicknesses, observed in human trachea (26). This simplified fluid transport model is consistent with our observations for mucus flows. However, we note that two factors remain missing from this simplified fluid model. First, it does not account for the effects of viscoelasticity, an important rheological component of mucus rheology. Second, it has been observed that mucus flows diminish at high viscoelasticities, presumably due to either limitations in the pumping shear stress available from cilia, or due to collapse of the ciliated layer (1, 19, 47).

We now turn to our observations of the cilia-generating pumping of the rotational flow pattern: the mucus hurricane. The cilia in the hurricane produce a circularly organized fluid flow (39); when the culture is tilted, the direction of the cilia-generated shear stress varies in its direction with respect to that of gravity. For example, when the channel is tilted vertically at 90°, cilia within regions of the hurricane push the overlying fluid downhill, adding to the effects of gravity, while on the opposing side of the hurricane, the cilia pump upward, against drainage. In contrast to what we observe empirically, the Blake et al. model (6) suggests that the net effect of gravity would be to displace the center of the hurricane downward with the same average velocity as the linear flows. This simplified insight ignores the fact that the rotational flow is specific to a particular region of the ciliation, and once the mucus has moved beyond this region of rotational organization, it would be subjected to shear stress applied by the new, local organization of cilia. Within the Blake model, the mucus hurricane offers a remarkable result.

Revisiting Blake's model, a 10-μm-thick, 2.5% reconstituted mucus layer would have a drainage rate of 0.7 μm/s at 45°. For the mucus hurricane data set, the system maintained a minimum 45° angle for 30 min (with most of the time being at 60° and 90°). For a drainage rate of 0.7 μm/s over 30 min, we would expect to see bead displacement of −1,200 μm. If we are more conservative with the liquid thickness and choose a depth of 2 μm, the minimum depth to submerge our beads, then we get a drainage rate of 50 μm over the course of 30 min. Remarkably, the hurricane showed no signs of drainage over the course of 30 min. To make the model consistent with our data, the viscosity of the fluid would have to approach that of COPD mucus (Fig. 7), which, in other reports, have resulted in stalled mucus flow (9, 45). We conclude that our observation of the absence of drainage in mucus hurricanes constitutes a remarkable failure of the shear flow boundary condition in cilia-generated flows of mucus.

The mucus hurricane's persistent transport suggests another interaction opposing gravity: we propose an adhesive interaction between the mucus and the epithelial surface that slows drainage rates. While mucoadhesion between the ASL and epithelium can inhibit transport in diseased states (37), it has also been speculated that adhesion between mucus and cilia may help to drive transport (50). This effective adhesion may be of a biochemical or a physical origin. Cilia penetration into the mucus mesh is a physical mechanism that may provide an effective adhesive interaction that could prevent mucus from draining. Understanding the exact nature of this interaction is key in not only determining the parameters that differentiate between healthy and unhealthy mucus, but also in potentially generating new approaches to treating failed mucociliary clearance (50).

The observation of buffer draining has implications for both the rheology and hydration of any fluid simulant. Bronchial periciliary layer fluid (PCL) drainage would dehydrate the ASL and increase adhesion between the ASL and epithelial surface.

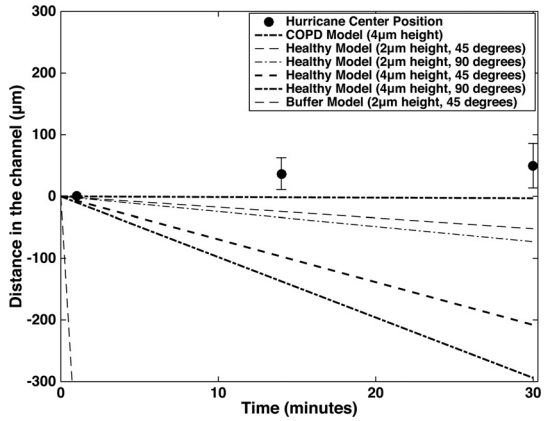

Fig. 7. The mucus hurricane does not drain in accordance with simple drainage models. The position of the mucus hurricane's center as a function of time is plotted along with drainage models for varying conditions. The buffer model refers to a 4-μm layer of PBS; the healthy model refers to 2.5% reconstituted mucus, with a nominal viscosity of 0.16 Pa·s; and the COPD model refers to a mucus with a viscosity of 10 Pa·s.

This dehydration and subsequent increase in adhesion leads to reduced MCC (48). Additionally, a 2010 Lee et al. article (34) uses a numerical model to predict that a PCL fluid depth shallower than the cilia height will reduce transport and ultimately render it ineffective.

Buffer also represents an interesting case in which the ASL may be too "thin" to effectively transport. Most clearance diseases are concerned with thickened mucus; however, a Rubin et al. (49) article attributes reduced clearance in the disease fucosidosis to thinned mucus. Thin mucus not transporting also has implications for mucolytic treatments (18). Mucolytics, agents that reduce the viscoelasticity of mucus by breaking bonds, have been used to treat several airway diseases. In a 1976 article, Puchelle et al. [(44), as cited in Ref. 22] observed that sputum with low "viscoelasticity" transported slowly on frog palate and cautioned against using mucolytics for patients with low viscoelasticity. Overtreating with mucolytics and excessively thinning the mucus would lead to a lack of vertical clearance. The MCAD serves as an ideal platform to test the effects of mucolytics on clearance.

Although we designed the MCAD to be a comprehensive platform to study mucociliary clearance as a function of gravitational drainage, there are some key limitations to our system. In basing our system on the ALI HBE culture model, we share many of its same strengths and weaknesses in regard to recreating the physiological environment of the lung. Although this culture model produces well-differentiated cultures (14) and the protein content of the secretions are similar to those found in vivo, there are important differences, many of which stem from the lack of contributions of submucosal glands and the peripheral lung compared with in vivo secretions (29). Submucosal secretions are of particular interest, as recent observations have shown morphological differences in mucus of submucosal origin (42), and the formation of a transporting "mucin-bundle" structure (11). We note that our primary contribution is to emphasize the importance of studying mucociliary clearance in the vertical direction, and this can be performed on a wide range of models, from our own cell culture model, to tissue slices, animals, and humans.

In the article presented here, we have developed the first cell culture assay system to explore the influence of gravity on mucociliary clearance. We integrated ciliated cells thriving within a microfluidics channel with a tilting microscope and tested the effects of gravity on mucociliary clearance. We found that buffer, which transported in a horizontal orientation, did not transport vertically against gravity. This finding establishes that gravity is an essential parameter in testing the biophysics driving mucus clearance. We also demonstrated that mucus does not drain at the rate predicted by simple models, and propose an adhesive interaction between the epithelial surface and the mucus as the reason for the reduced drainage. Finally, the MCAD can be used as a tool to select for the rheological and biochemical properties that enable mucus to transport against gravity in vivo, as well as the impact of mucolytic treatments on effective vertical clearance.

ACKNOWLEDGMENTS

We thank the University of North Carolina (UNC) Cystic Fibrosis Tissue Culture Core for providing both cells and media. We thank the UNC Physics Machine Shop for machining components of our microscope. We also thank the Chapel Hill Analytical and Nanofabrication Laboratory for assistance with photolithography and nanofabrication.

GRANTS

This work was supported by the National Institutes of Health Grant P41-EB002025-34.

DISCLOSURES

No conflicts of interest, financial or otherwise, are declared by the authors.

AUTHOR CONTRIBUTIONS

J.C. and R.S. conceived and designed research; J.C., S.E.L., J.A.C., S.K., and D.B.H. performed experiments; J.C., S.E.L., and J.A.C. analyzed data; J.C. and R.S. interpreted results of experiments; J.C. prepared figures; J.C. drafted manuscript; J.C., J.A.C., D.B.H., and R.S. edited and revised manuscript; J.C., D.B.H., and R.S. approved final version of manuscript.

REFERENCES

1. **Anderson WH, Coakley RD, Button B, Henderson AG, Zeman KL, Alexis NE, Peden DB, Lazarowski ER, Davis CW, Bailey S, Fuller F, Almond M, Qaqish B, Bordonali E, Rubinstein M, Bennett WD, Kesimer M, Boucher RC.** The relationship of mucus concentration (hydration) to mucus osmotic pressure and transport in chronic bronchitis. *Am J Respir Crit Care Med* 192: 182–190, 2015. doi:10.1164/rccm.201412-2230OC.
2. **Ballard ST, Parker JC, Hamm CR.** Restoration of mucociliary transport in the fluid-depleted trachea by surface-active instillates. *Am J Respir Cell Mol Biol* 34: 500–504, 2006. doi:10.1165/rcmb.2005-0214OC.
3. **Benam KH, Villenave R, Lucchesi C, Varone A, Hubeau C, Lee HH, Alves SE, Salmon M, Ferrante TC, Weaver JC, Bahinski A, Hamilton GA, Ingber DE.** Small airway-on-a-chip enables analysis of human lung inflammation and drug responses in vitro. *Nat Methods* 13: 151–157, 2016. doi:10.1038/nmeth.3697.
4. **Bermbach S, Weinhold K, Roeder T, Petersen F, Kugler C, Goldmann T, Rupp J, König P.** Mechanisms of cilia-driven transport in the airways in the absence of mucus. *Am J Respir Cell Mol Biol* 51: 56–67, 2014. doi:10.1165/rcmb.2012-0530OC.
5. **Bernacki SH, Nelson AL, Abdullah L, Sheehan JK, Harris A, Davis CW, Randell SH.** Mucin gene expression during differentiation of human airway epithelia in vitro. Muc4 and muc5b are strongly induced. *Am J Respir Cell Mol Biol* 20: 595–604, 1999. doi:10.1165/ajrcmb.20.4.3442.
6. **Blake J.** Mucus flows. *Math Biosci* 17: 301–313, 1973. doi:10.1016/0025-5564(73)90073-4.
7. **Bonser LR, Zlock L, Finkbeiner W, Erle DJ.** Epithelial tethering of MUC5AC-rich mucus impairs mucociliary transport in asthma. *J Clin Invest* 126: 2367–2371, 2016. doi:10.1172/JCI84910.
8. **Button B, Cai LH, Ehre C, Kesimer M, Hill DB, Sheehan JK, Boucher RC, Rubinstein M.** A periciliary brush promotes the lung health by separating the mucus layer from airway epithelia. *Science* 337: 937–941, 2012. doi:10.1126/science.1223012.
9. **Chen TM, Dulfano MJ.** Mucus viscoelasticity and mucociliary transport rate. *J Lab Clin Med* 91: 423–431, 1978.
10. **Chernov N.** Ellipse fit (direct method). https://www.mathworks.com/matlabcentral/fileexchange/22684-ellipse-fit-direct-method 2009.
11. **Ermund A, Meiss LN, Rodriguez-Pineiro AM, Bähr A, Nilsson HE, Trillo-Muyo S, Ridley C, Thornton DJ, Wine JJ, Hebert H, Klymiuk N, Hansson GC.** The normal trachea is cleaned by MUC5B mucin bundles from the submucosal glands coated with the MUC5AC mucin. *Biochem Biophys Res Commun* 492: 331–337, 2017. doi:10.1016/j.bbrc.2017.08.113.
12. **Even-Tzur N, Elad D, Zaretsky U, Randell SH, Haklai R, Wolf M.** Custom-designed wells and flow chamber for exposing air-liquid interface cultures to wall shear stress. *Ann Biomed Eng* 34: 1890–1895, 2006. doi:10.1007/s10439-006-9211-8.
13. **Freitas DA, Dias FA, Chaves GS, Ferreira GM, Ribeiro CT, Guerra RO, Mendonça KM.** Standard (head-down tilt) versus modified (without head-down tilt) postural drainage in infants and young children with cystic fibrosis. *Cochrane Database Syst Rev* 157: CD010297, 2015. doi:10.1002/14651858.CD010297.pub2.
14. **Fulcher ML, Gabriel S, Burns KA, Yankaskas JR, Randell SH.** Well-differentiated human airway epithelial cell cultures. *Methods Mol Med* 107: 183–206, 2005.
15. **Gelman RA, Meyer FA.** Mucociliary transference rate and mucus viscoelasticity dependence on dynamic storage and loss modulus. *Am Rev Respir Dis* 120: 553–557, 1979.

16. **Gray TE, Guzman K, Davis CW, Abdullah LH, Nettesheim P.** Mucociliary differentiation of serially passaged normal human tracheobronchial epithelial cells. *Am J Respir Cell Mol Biol* 14: 104–112, 1996. doi:10.1165/ajrcmb.14.1.8534481.
17. **Halır R, Flusser J.** Numerically stable direct least squares fitting of ellipses. In: *Proceedings of the 6th International Conference in Central Europe on Computer Graphics and Visualization.* Plzen, Czech Republic: World Society for Computer Graphics, 1998, p. 125–132.
18. **Henke MO, Ratjen F.** Mucolytics in cystic fibrosis. *Paediatr Respir Rev* 8: 24–29, 2007. doi:10.1016/j.prrv.2007.02.009.
19. **Hill DB, Swaminathan V, Estes A, Cribb J, O'Brien ET, Davis CW, Superfine R.** Force generation and dynamics of individual cilia under external loading. *Biophys J* 98: 57–66, 2010. doi:10.1016/j.bpj.2009.09.048.
20. **Hill DB, Vasquez PA, Mellnik J, McKinley SA, Vose A, Mu F, Henderson AG, Donaldson SH, Alexis NE, Boucher RC, Forest MG.** A biophysical basis for mucus solids concentration as a candidate biomarker for airways disease. *PLoS One* 9: e87681, 2014. [Erratum in *PLoS One* 9: e97980, 2014.] doi:10.1371/journal.pone.0087681.
21. **Hoegger MJ, Fischer AJ, McMenimen JD, Ostedgaard LS, Tucker AJ, Awadalla MA, Moninger TO, Michalski AS, Hoffman EA, Zabner J, Stoltz DA, Welsh MJ.** Impaired mucus detachment disrupts mucociliary transport in a piglet model of cystic fibrosis. *Science* 345: 818–822, 2014. doi:10.1126/science.1255825.
22. **Houtmeyers E, Gosselink R, Gayan-Ramirez G, Decramer M.** Effects of drugs on mucus clearance. *Eur Respir J* 14: 452–467, 1999. doi:10.1034/j.1399-3003.1999.14b35.x.
23. **Huh D, Fujioka H, Tung YC, Futai N, Paine R 3rd, Grotberg JB, Takayama S.** Acoustically detectable cellular-level lung injury induced by fluid mechanical stresses in microfluidic airway systems. *Proc Natl Acad Sci USA* 104: 18886–18891, 2007. doi:10.1073/pnas.0610868104.
24. **Huh D, Matthews BD, Mammoto A, Montoya-Zavala M, Hsin HY, Ingber DE.** Reconstituting organ-level lung functions on a chip. *Science* 328: 1662–1668, 2010. doi:10.1126/science.1188302.
25. **Hussong J, Lindken R, Faulhammer P, Noreikat K, Sharp KV, Kummer W, Westerweel J.** Cilia-driven particle and fluid transport over mucus-free mice tracheae. *J Biomech* 46: 593–598, 2013. doi:10.1016/j.jbiomech.2012.08.020.
26. **Jayaraman S, Song Y, Vetrivel L, Shankar L, Verkman AS.** Noninvasive in vivo fluorescence measurement of airway-surface liquid depth, salt concentration, and pH. *J Clin Invest* 107: 317–324, 2001. doi:10.1172/JCI11154.
27. **Jeong JH, Joo NS, Hwang PH, Wine JJ.** Mucociliary clearance and submucosal gland secretion in the ex vivo ferret trachea. *Am J Physiol Lung Cell Mol Physiol* 307: L83–L93, 2014. doi:10.1152/ajplung.00009.2014.
28. **Kesimer M, Ehre C, Burns KA, Davis CW, Sheehan JK, Pickles RJ.** Molecular organization of the mucins and glycocalyx underlying mucus transport over mucosal surfaces of the airways. *Mucosal Immunol* 6: 379–392, 2013. doi:10.1038/mi.2012.81.
29. **Kesimer M, Kirkham S, Pickles RJ, Henderson AG, Alexis NE, Demaria G, Knight D, Thornton DJ, Sheehan JK.** Tracheobronchial air-liquid interface cell culture: a model for innate mucosal defense of the upper airways? *Am J Physiol Lung Cell Mol Physiol* 296: L92–L100, 2009. doi:10.1152/ajplung.90388.2008.
30. **King M.** Relationship between mucus viscoelasticity and ciliary transport in guaran gel/frog palate model system. *Biorheology* 17: 249–254, 1980.
31. **King M, Brock G, Lundell C.** Clearance of mucus by simulated cough. *J Appl Physiol (1985)* 58: 1776–1782, 1985. doi:10.1152/jappl.1985.58.6.1776.
32. **Knowles MR, Boucher RC.** Mucus clearance as a primary innate defense mechanism for mammalian airways. *J Clin Invest* 109: 571–577, 2002. doi:10.1172/JCI0215217.
33. **Lannefors L, Wollmer P.** Mucus clearance with three chest physiotherapy regimes in cystic fibrosis: a comparison between postural drainage, PEP and physical exercise. *Eur Respir J* 5: 748–753, 1992.
34. **Lee WL, Jayathilake PG, Tan Z, Le DV, Lee HP, Khoo BC.** Muco-ciliary transport: Effect of mucus viscosity, cilia beat frequency and cilia density. *Comp Fluids* 49: 214–221, 2011. doi:10.1016/j.compfluid.2011.05.016.
35. **Liu L, Shastry S, Byan-Parker S, Houser G, K Chu K, Birket SE, Fernandez CM, Gardecki JA, Grizzle WE, Wilsterman EJ, Sorscher EJ, Rowe SM, Tearney GJ.** An autoregulatory mechanism governing mucociliary transport is sensitive to mucus load. *Am J Respir Cell Mol Biol* 51: 485–493, 2014. doi:10.1165/rcmb.2013-0499MA.
36. **Liu T, Moiseeva E. Harnett CK.** Integrated reservoirs for PDMS microfluidic chips, Chips & Tips. *Lab Chip* April 22, 2008.
37. **Mall M, Grubb BR, Harkema JR, O'Neal WK, Boucher RC.** Increased airway epithelial Na^+ absorption produces cystic fibrosis-like lung disease in mice. *Nat Med* 10: 487–493, 2004. doi:10.1038/nm1028.
38. **Mathers C, Fat DM, Boerma JT.** *The Global Burden of Disease: 2004 Update*. Geneva, Switzerland: WHO, 2008.
39. **Matsui H, Randell SH, Peretti SW, Davis CW, Boucher RC.** Coordinated clearance of periciliary liquid and mucus from airway surfaces. *J Clin Invest* 102: 1125–1131, 1998. doi:10.1172/JCI2687.
40. **Naylor JM, McLean A, Chow C-M, Heard R, Ting I, Avolio A.** A modified postural drainage position produces less cardiovascular stress than a head-down position in patients with severe heart disease: a quasi-experimental study. *Aust J Physiother* 52: 201–209, 2006. doi:10.1016/S0004-9514(06)70029-0.
41. **Norton MM, Robinson RJ, Weinstein SJ.** Model of ciliary clearance and the role of mucus rheology. *Phys Rev E Stat Nonlin Soft Matter Phys* 83: 011921, 2011. doi:10.1103/PhysRevE.83.011921.
42. **Ostedgaard LS, Moninger TO, McMenimen JD, Sawin NM, Parker CP, Thornell IM, Powers LS, Gansemer ND, Bouzek DC, Cook DP, Meyerholz DK, Abou Alaiwa MH, Stoltz DA, Welsh MJ.** Gel-forming mucins form distinct morphologic structures in airways. *Proc Natl Acad Sci USA* 114: 6842–6847, 2017. doi:10.1073/pnas.1703228114.
43. **Ostrowski LE, Yin W, Rogers TD, Busalacchi KB, Chua M, O'Neal WK, Grubb BR.** Conditional deletion of dnaic1 in a murine model of primary ciliary dyskinesia causes chronic rhinosinusitis. *Am J Respir Cell Mol Biol* 43: 55–63, 2010. doi:10.1165/rcmb.2009-0118OC.
44. **Puchelle E, Girard F, Zahm JM.** Rheology of bronchial secretions and mucociliary transport (author's transl). [French] *Bull Eur Physiopathol Respir* 12: 771–779, 1976.
45. **Puchelle E, Zahm JM, Quemada D.** Rheological properties controlling mucociliary frequency and respiratory mucus transport. *Biorheology* 24: 557–563, 1987. doi:10.3233/BIR-1987-24606.
46. **Puchelle E, Zahm JM, Sadoul P.** Mucociliary frequency of frog palate epithelium. *Am J Physiol Cell Physiol* 242: C31–C35, 1982. doi:10.1152/ajpcell.1982.242.1.C31.
47. **Puchelle E, Zahm JM.** Influence of rheological properties of human bronchial secretions on the ciliary beat frequency. *Biorheology* 21: 265–272, 1984. doi:10.3233/BIR-1984-211-228.
48. **Randell SH, Boucher RC; University of North Carolina Virtual Lung Group.** Effective mucus clearance is essential for respiratory health. *Am J Respir Cell Mol Biol* 35: 20–28, 2006. doi:10.1165/rcmb.2006-0082SF.
49. **Rubin BK, MacLeod PM, Sturgess J, King M.** Recurrent respiratory infections in a child with fucosidosis: is the mucus too thin for effective transport? *Pediatr Pulmonol* 10: 304–309, 1991. doi:10.1002/ppul.1950100415.
50. **Sears PR, Davis CW, Chua M, Sheehan JK.** Mucociliary interactions and mucus dynamics in ciliated human bronchial epithelial cell cultures. *Am J Physiol Lung Cell Mol Physiol* 301: L181–L186, 2011. doi:10.1152/ajplung.00321.2010.
51. **Sellgren KL, Butala EJ, Gilmour BP, Randell SH, Grego S.** A biomimetic multicellular model of the airways using primary human cells. *Lab Chip* 14: 3349–3358, 2014. doi:10.1039/C4LC00552J.
52. **Shields AR, Fiser BL, Evans BA, Falvo MR, Washburn S, Superfine R.** Biomimetic cilia arrays generate simultaneous pumping and mixing regimes. *Proc Natl Acad Sci USA* 107: 15670–15675, 2010. doi:10.1073/pnas.1005127107.
53. **Smith DJ, Gaffney EA, Blake JR.** A viscoelastic traction layer model of muco-ciliary transport. *Bull Math Biol* 69: 289–327, 2007. doi:10.1007/s11538-006-9177-6.
54. **Weibel ER, Gomez DM.** Architecture of the human lung. Use of quantitative methods establishes fundamental relations between size and number of lung structures. *Science* 137: 577–585, 1962. doi:10.1126/science.137.3530.577.
55. **Wong JW, Keens TG, Wannamaker EM, Crozier DN, Levison H, Aspin N.** Effects of gravity on tracheal mucus transport rates in normal subjects and in patients with cystic fibrosis. *Pediatrics* 60: 146–152, 1977.
56. **Zhou Z, Duerr J, Johannesson B, Schubert SC, Treis D, Harm M, Graeber SY, Dalpke A, Schultz C, Mall MA.** The ENaC-overexpressing mouse as a model of cystic fibrosis lung disease. *J Cyst Fibros* 10, *Suppl* 2: S172–S182, 2011. doi:10.1016/S1569-1993(11)60021-0.